

**FABRICATION AND CHARACTERIZATION OF
POLY(3-HYDROXYBUTYRATE-*co*-4-
HYDROXYBUTYRATE)/CHITOSAN BLEND AND
ITS SILVER NANOCOMPOSITE MATERIAL**

RENNUKKA A/P MATHAVA

**UNIVERSITI SAINS MALAYSIA
2014**

**FABRICATION AND CHARACTERIZATION OF
POLY(3-HYDROXYBUTYRATE-*co*-4-
HYDROXYBUTYRATE)/CHITOSAN BLEND AND
ITS SILVER NANOCOMPOSITE MATERIAL**

by

RENNUKKA A/P MATHAVA

**Thesis submitted in fulfilment of the requirements
for the degree of
Master of Science**

February 2014

ACKNOWLEDGEMENTS

The success of my research would not be possible without the guidance and support of several individuals who directly or indirectly contributed and extended their invaluable assistance in the preparation and completion of this study. First and foremost, I am thankful to God who continuously showered me with blessings and courage throughout my project. My sincere gratitude goes to my supervisor, Assoc. Prof. Dr. Amirul Al Ashraf Abdullah for his immense knowledge, patience, enthusiasm and helpful suggestions in helping me all the time of my research and writing of this thesis.

I am indebted to my father, mother, sisters and Mr. Harridas who have given me their unconditional love and personal support. They have been my core strength in overcoming the obstacles in my daily routine of research life. My journey would not be complete without these individual's encouragement and motivation. Next, I would like to convey my special thanks to Ms. Hema, Ms. Shantini, Ms. Solehah, Ms. Vigneswari, Ms. Hemalatha, Ms. Syairah, Ms. Faezah, Ms. Hezreen, Ms. Zai and all Lab 318 members for sharing their knowledge and giving me moral support during the hard time of my project.

Finally, I would like to express my heartfelt thanks to Mr. Zahari, Mr. Sekaran and other lab assistances who willingly helped me in my research activities. Besides that, I wish to avail myself in this opportunity to extend my sincere thanks to Electron microscope staffs especially Mr. Johari and Ms. Jamilah for their assistance. Lastly, I am grateful to School of Chemistry and Physics who allowed me to utilize their research facilities. Last but not least, I really appreciated Universiti Sains Malaysia and government for awarding me with the USM fellowship and MyMaster scholarship.

TABLE OF CONTENTS

	PAGES
ACKNOWLEDGEMENTS	ii
TABLE OF CONTENTS	iii
LIST OF TABLES	viii
LIST OF FIGURES	xi
LIST OF APPENDICES	xv
LIST OF SYMBOLS AND ABBREVIATIONS	xvi
ABSTRAK	xxiii
ABSTRACT	xxv
1.0 INTRODUCTION	1
2.0 LITERATURE REVIEW	5
2.1 Polyhydroxyalkanoate (PHA)	5
2.1.1 Poly(3-hydroxybutyrate) [P(3HB)]	8
2.1.2 Poly(4-hydroxybutyrate) [P(4HB)]	11
2.1.3 Poly(3-hydroxybutyrate- <i>co</i> -4-hydroxybutyrate) [P(3HB- <i>co</i> -4HB)]	13
2.2 Chitosan (CS)	17
2.3 Blending polymers from renewable resources (PFRR)	20
2.3.1 Solution blending	22
2.3.2 Modification of polymer blend via cross-linking	22
2.4 Nanotechnology and nanocomposites	26
2.4.1 Silver nanoparticle (SNP) and its emerging antibacterial property	29
2.5 The outlook of P(3HB- <i>co</i> -4HB) based blends and nanocomposites	32

2.6	Concluding remarks	34
3.0	MATERIALS AND METHODS	36
3.1	General techniques	36
3.2	Determination of bacterial growth	36
3.3	Centrifugation of culture	37
3.4	Freeze drying	37
3.5	Bacterial strain and maintenance	37
3.6	Preparation of media and buffer	38
	3.6.1 Nutrient agar (NA) medium	38
	3.6.2 Nutrient rich (NR) broth	38
	3.6.3 PHA biosynthesis medium for modified two-stage cultivation	39
	3.6.4 Preparation of phosphate buffered saline (PBS)	39
3.7	PHA biosynthesis	40
	3.7.1 Preculture preparation	40
	3.7.2 Biosynthesis of P(3HB- <i>co</i> -4HB) copolymer by <i>Cupriavidus</i> sp. USMAA1020 in 15 L fermenter	40
3.8	Extraction of P(3HB- <i>co</i> -4HB) from the freeze dried cells	41
3.9	Fabrication of copolymer, blend and nanocomposite films	42
	3.9.1 Fabrication of P(3HB- <i>co</i> -4HB) films via solvent casting method	42
	3.9.2 Fabrication of P(3HB- <i>co</i> -4HB)/chitosan blend films via solvent blending method	42
	3.9.3 Cross-linking of P(3HB- <i>co</i> -4HB)/chitosan blend films	43
	3.9.4 Fabrication of P(3HB- <i>co</i> -4HB)/chitosan/silver nanocomposite films	43
3.10	Characterization of the copolymer, blend and nanocomposite films	44

3.10.1	Fourier transform infrared spectroscopy (FTIR)	44
3.10.2	Ionic exchange capacity (IEC)	44
3.10.3	Film solubility and water absorption capacity	45
3.10.4	Scanning electron microscopy (SEM)	45
3.10.5	Atomic force microscopy (AFM)	46
3.10.6	Tensile test	46
3.10.7	Differential scanning calorimeter (DSC)	47
3.10.8	Thermogravimetric analysis (TGA)	47
3.10.9	X-ray diffraction (XRD)	47
3.11	<i>In vitro</i> antibacterial assessment	48
3.11.1	Disc diffusion (Qualitative method)	48
3.11.2	Colony count (Quantitative method)	48
3.12	<i>In vitro</i> biodegradation test	49
3.13	Statistical analysis	49
3.14	Analytical method	50
3.14.1	Gas chromatography (GC) analysis	50
4.0	RESULTS AND DISCUSSION	52
4.1	Biosynthesis of P(3HB- <i>co</i> -4HB) copolymer via a modified two stage cultivation method	52
4.2	Fabrication of P(3HB- <i>co</i> -4HB)/chitosan blend films via solvent blending method	58
4.3	Characterization of P(3HB- <i>co</i> -4HB)/chitosan blend films from solvent blending method	59
4.3.1	Fourier transform infrared (FTIR) analysis	59
4.3.2	Film solubility and water absorption capacity	65
4.3.3	Surface morphology	71
4.3.4	Mechanical properties	81

4.3.5	Thermal properties	83
4.3.6	<i>In vitro</i> antimicrobial activity of the blend films	87
4.4	Fabrication of the P(3HB- <i>co</i> -4HB)/20 wt% chitosan blend films via chemical cross-linking method	92
4.5	Characterization of chemically cross-linked P(3HB- <i>co</i> -4HB)/20 wt% chitosan blend films	93
4.5.1	Structural analysis by Fourier transform infrared (FTIR) studies and extent of cross-linking via ionic exchange capacity (IEC) method	93
4.5.2	Film solubility and water absorption capacity	103
4.5.3	Surface morphology	107
4.5.4	Mechanical properties	113
4.5.5	Thermal properties	116
4.5.6	<i>In vitro</i> antimicrobial activity of the cross-linked blend films	119
4.6	Fabrication of cross-linked P(3HB- <i>co</i> -44%4HB)/20 wt% chitosan incorporated with different contents of silver nanoparticle (SNP)	123
4.7	Characterization of cross-linked P(3HB- <i>co</i> -44%4HB)/20 wt% chitosan incorporated with different contents of silver nanoparticle (SNP)	124
4.7.1	Fourier transform infrared (FTIR) analysis of the nanocomposite films	124
4.7.2	X-ray diffraction (XRD) analysis of the nanocomposite films	126
4.7.3	Surface morphology of the nanocomposite films	130
4.7.4	Mechanical properties of the nanocomposite films	135
4.7.5	Thermal properties of the nanocomposite films	137
4.7.6	Assessment of antimicrobial activity of the nanocomposite films	139
4.8	Biodegradability of the P(3HB- <i>co</i> -44%4HB), P(3HB- <i>co</i> -44%4HB)/20 wt% chitosan blend film cross-linked with 5% (w/v) of	146

glutaraldehyde and its silver nanocomposite films

5.0	CONCLUSIONS	151
6.0	FUTURE RECOMMENDATIONS	153
	REFERENCES	155
	APPENDICES	
	LIST OF PUBLICATIONS AND CONFERENCES	

LIST OF TABLES

	PAGES	
Table 2.1:	The general differences between P(4HB) and PGA	12
Table 2.2:	Thermal properties of different compositions of P(3HB- <i>co</i> -4HB) copolymer	14
Table 3.1:	Materials that were required for the preparation of 1 L of NA	38
Table 3.2:	Materials that were required for the preparation of 1 L of NR	38
Table 3.3:	Materials of trace elements that were dissolved in 1 L of hydrochloric acid (0.1 M)	39
Table 3.4:	Materials that were required for the preparation of PBS (0.1 M)	40
Table 3.5:	Manipulation of different carbon sources and concentrations to obtain the desired copolymer compositions	41
Table 3.6:	Several parts of the machine and operation programmes that were important for the GC analysis	51
Table 4.1:	Effect of chitosan content on the solubility of the films	66
Table 4.2:	Pore size of the P(3HB- <i>co</i> -4HB)/chitosan blend films	73
Table 4.3:	Surface roughness of the P(3HB- <i>co</i> -4HB) copolymers and their blend films incorporated with different contents of chitosan	80
Table 4.4:	Mechanical properties of the P(3HB- <i>co</i> -4HB) copolymers and their blend films	82
Table 4.5:	Thermal characteristics of chitosan, pure copolymers and blend films with various contents of chitosan based on the thermograms	84
Table 4.6:	Antimicrobial performance of the blend films via disc diffusion method against <i>Escherichia coli</i> and <i>Staphylococcus aureus</i>	88
Table 4.7:	Antimicrobial activity of the blend films via colony count method against <i>Escherichia coli</i>	89
Table 4.8:	Antimicrobial activity of the blend films via colony count method against <i>Staphylococcus aureus</i>	90

Table 4.9:	Ionic exchange capacity of the P(3HB- <i>co</i> -4HB)/20 wt% chitosan blend films cross-linked with different concentrations of glutaraldehyde	102
Table 4.10:	Film solubility of the P(3HB- <i>co</i> -4HB)/20 wt% chitosan blend films cross-linked by different concentrations of glutaraldehyde	104
Table 4.11:	Pore size of the P(3HB- <i>co</i> -4HB)/20 wt% chitosan blend films cross-linked with 5% (w/v) of glutaraldehyde	109
Table 4.12:	Surface roughness of the blend films with 20 wt% of chitosan cross-linked with 5% (w/v) of glutaraldehyde	112
Table 4.13:	Mechanical properties of the P(3HB- <i>co</i> -4HB)/20 wt% chitosan blend films cross-linked with different concentrations of glutaraldehyde	114
Table 4.14:	Thermal properties and stability of the P(3HB- <i>co</i> -4HB)/20 wt% chitosan blend films cross-linked with different concentrations of glutaraldehyde	117
Table 4.15:	Qualitative assessment of the P(3HB- <i>co</i> -44%4HB)/20 wt% chitosan blend films cross-linked with different concentrations of glutaraldehyde against <i>Escherichia coli</i> and <i>Staphylococcus aureus</i>	120
Table 4.16:	Antimicrobial activity of the P(3HB- <i>co</i> -44%4HB)/20 wt% chitosan blend films cross-linked with different concentrations of glutaraldehyde via colony count method against <i>Escherichia coli</i>	121
Table 4.17:	Antimicrobial activity of the P(3HB- <i>co</i> -44%4HB)/20 wt% chitosan blend films cross-linked with different concentrations of glutaraldehyde via colony count method against <i>Staphylococcus aureus</i>	122
Table 4.18:	XRD studies of nanocomposite films of the P(3HB- <i>co</i> -44%4HB)/20 wt% chitosan cross-linked with 5% (w/v) of glutaraldehyde	128
Table 4.19:	Surface roughness of nanocomposite films of the P(3HB- <i>co</i> -44%4HB)/20 wt% chitosan cross-linked with 5% (w/v) of glutaraldehyde incorporated with different contents of SNP	134
Table 4.20:	Mechanical properties of nanocomposite films of the P(3HB- <i>co</i> -44%4HB)/20 wt% chitosan cross-linked with 5% (w/v) of glutaraldehyde incorporated with different contents of SNP	136

Table 4.21:	Thermal properties of nanocomposite films of the P(3HB- <i>co</i> -44%4HB)/20 wt% chitosan cross-linked with 5% (w/v) of glutaraldehyde incorporated with different contents of SNP	138
Table 4.22:	Qualitative assessment of nanocomposite films of the P(3HB- <i>co</i> -44%4HB)/20 wt% chitosan cross-linked with 5% (w/v) of glutaraldehyde incorporated with different contents of SNP	140
Table 4.23:	Antimicrobial activity via colony count method of nanocomposite films of the P(3HB- <i>co</i> -44%4HB)/20 wt% chitosan cross-linked with 5% (w/v) of glutaraldehyde incorporated with different contents of SNP against <i>Escherichia coli</i>	141
Table 4.24:	Antimicrobial activity via colony count method of nanocomposite films of the P(3HB- <i>co</i> -44%4HB)/20 wt% chitosan cross-linked with 5% (w/v) of glutaraldehyde incorporated with different contents of SNP against <i>Pseudomonas aeruginosa</i>	142
Table 4.25:	Antimicrobial activity via colony count method of nanocomposite films of the P(3HB- <i>co</i> -44%4HB)/20 wt% chitosan cross-linked with 5% (w/v) of glutaraldehyde incorporated with different contents of SNP against <i>Staphylococcus aureus</i>	143
Table 4.26:	Antimicrobial activity via colony count method of nanocomposite films of the P(3HB- <i>co</i> -44%4HB)/20 wt% chitosan cross-linked with 5% (w/v) of glutaraldehyde incorporated with different contents of SNP against <i>Bacillus subtilis</i>	144

LIST OF FIGURES

	PAGES
Figure 2.1: Chemical structure of the PHA	6
Figure 2.2: The three step biosynthesis pathway of P(3HB)	10
Figure 2.3: Biosynthesis pathway of P(3HB-co-4HB) from different carbon precursors	16
Figure 2.4: Structure of chitin and chitosan	18
Figure 2.5: Classification of the biopolymers from three different sources	21
Figure 2.6: Structure of polymer network	23
Figure 2.7: The three different types of nanoparticles	27
Figure 2.8: Illustration of polymer-inorganic nanocomposite material connected by van der Waals force or hydrogen bonds	28
Figure 2.9: Multiple bactericidal actions of the silver nanoparticle (SNP)	30
Figure 4.1: Growth of <i>Cupriavidus</i> sp. USMAA1020 and PHA production profile of P(3HB-co-10%4HB) copolymer through modified two-stage cultivation	54
Figure 4.2: Growth <i>Cupriavidus</i> sp. USMAA1020 and PHA production profile of P(3HB-co-18%4HB) copolymer through modified two-stage cultivation	54
Figure 4.3: Growth <i>Cupriavidus</i> sp. USMAA1020 and PHA production profile of P(3HB-co-28%4HB) copolymer through modified two-stage cultivation	55
Figure 4.4: Growth <i>Cupriavidus</i> sp. USMAA1020 and PHA production profile of P(3HB-co-44%4HB) copolymer through modified two-stage cultivation	55
Figure 4.5: FTIR spectra of chitosan (a), P(3HB-co-10%4HB) (b) and blend films incorporated with 5 (c) and 20 (d) wt% chitosan	60
Figure 4.6: FTIR spectra of P(3HB-co-18%4HB) (a) and blend films incorporated with 5 (b) and 20 (c) wt% chitosan	61
Figure 4.7: FTIR spectra of P(3HB-co-28%4HB) (a) and blend films incorporated with 5 (b) and 20 (c) wt% chitosan	62

Figure 4.8:	FTIR spectra of P(3HB- <i>co</i> -44%4HB) (a) and blend films incorporated with 5 (b) and 20 (c) wt% chitosan	63
Figure 4.9:	Water absorption capacity of the P(3HB- <i>co</i> -10%4HB) blend films with different contents of chitosan	68
Figure 4.10:	Water absorption capacity of the P(3HB- <i>co</i> -18%4HB) blend films with different contents of chitosan	68
Figure 4.11:	Water absorption capacity of the P(3HB- <i>co</i> -28%4HB) blend films with different contents of chitosan	69
Figure 4.12:	Water absorption capacity of the P(3HB- <i>co</i> -44%4HB) blend films with different contents of chitosan	69
Figure 4.13:	Surface morphology of P(3HB- <i>co</i> -10%4HB) (a), P(3HB- <i>co</i> -18%4HB) (b), P(3HB- <i>co</i> -28%4HB) (c), P(3HB- <i>co</i> -44%4HB) (d) and blend films incorporated with 5 (e, f, g & h) and 20 (i, j, k & l) wt% of chitosan under 100× magnification	72
Figure 4.14:	AFM topographic images of P(3HB- <i>co</i> -10%4HB) (a, b) and blend films with 5 (c, d) and 20 (e, f) wt% chitosan and its three dimensional images (b, d & f)	76
Figure 4.15:	AFM topographic images of P(3HB- <i>co</i> -18%4HB) (a, b) and blend films with 5 (c, d) and 20 (e, f) wt% chitosan and its three dimensional images (b, d & f).	77
Figure 4.16:	AFM topographic images of P(3HB- <i>co</i> -28%4HB) (a, b) and blend films with 5 (c, d) and 20 (e, f) wt% chitosan and its three dimensional images (b, d & f)	78
Figure 4.17:	AFM topographic images of P(3HB- <i>co</i> -44%4HB) (a, b) and blend films with 5 (c, d) and 20 (e, f) wt% chitosan and its three dimensional images (b, d & f)	79
Figure 4.18:	Proposed structures of P(3HB- <i>co</i> -4HB)/chitosan blend films cross-linked with glutaraldehyde	94
Figure 4.19:	FTIR spectra of the P(3HB- <i>co</i> -10%4HB) blend films with 20 wt% chitosan cross-linked with 1 (a), 3 (b) and 5 (c) % (w/v) of glutaraldehyde	96
Figure 4.20:	FTIR spectra of the P(3HB- <i>co</i> -18%4HB) blend films with 20 wt% chitosan cross-linked with 1 (a), 3 (b) and 5 (c) % (w/v) of glutaraldehyde	97
Figure 4.21:	FTIR spectra of the P(3HB- <i>co</i> -28%4HB) blend films with 20 wt% chitosan cross-linked with 1 (a), 3 (b) and 5 (c) % (w/v) of glutaraldehyde	98

Figure 4.22:	FTIR spectra of the P(3HB- <i>co</i> -44%4HB) blend films with 20 wt% chitosan cross-linked with 1 (a), 3 (b) and 5 (c) % (w/v) of glutaraldehyde	99
Figure 4.23:	Water absorption capacity of the P(3HB- <i>co</i> -10%4HB)/20 wt% chitosan blend films cross-linked using different concentrations of glutaraldehyde [% (w/v)]	105
Figure 4.24:	Water absorption capacity of the P(3HB- <i>co</i> -18%4HB)/20 wt% chitosan blend films cross-linked using different concentrations of glutaraldehyde [% (w/v)]	105
Figure 4.25:	Water absorption capacity of the P(3HB- <i>co</i> -28%4HB)/20 wt% chitosan blend films cross-linked using different concentrations of glutaraldehyde [% (w/v)]	106
Figure 4.26:	Water absorption capacity of the P(3HB- <i>co</i> -44%4HB)/20 wt% chitosan blend films cross-linked using different concentrations of glutaraldehyde [% (w/v)]	106
Figure 4.27:	Surface morphology of the P(3HB- <i>co</i> -10%4HB) (a), P(3HB- <i>co</i> -18%4HB) (b), P(3HB- <i>co</i> -28%4HB) (c) and P(3HB- <i>co</i> -44%4HB) (d) blend films with 20 wt% of chitosan cross-linked with 5% (w/v) of glutaraldehyde under 100× magnification	108
Figure 4.28:	AFM topographic images of P(3HB- <i>co</i> -10%4HB) (a), P(3HB- <i>co</i> -18%4HB) (b), P(3HB- <i>co</i> -28%4HB) (c), P(3HB- <i>co</i> -44%4HB) (d) blend films with 20 wt% of chitosan cross-linked with 5% (w/v) of glutaraldehyde and its three dimensional images (e, f, g & h)	111
Figure 4.29:	FTIR spectra of nanocomposite films of the P(3HB- <i>co</i> -44%4HB)/20 wt% chitosan cross-linked with 5% (w/v) glutaraldehyde incorporated with 1 (a), 5 (b) and 9 (c) wt% of SNP	125
Figure 4.30:	XRD patterns of the cross-linked P(3HB- <i>co</i> -44%4HB)/20 wt% chitosan (a), SNP (b) and its nanocomposite films incorporated with 1 (c), 5 (d) and 9 (e) wt% of SNP	127
Figure 4.31:	Surface morphology and elemental mapping of nanocomposite films of the P(3HB- <i>co</i> -44%4HB)/20 wt% chitosan cross-linked with 5% (w/v) of glutaraldehyde incorporated with 1 (a), 3 (b), 5 (c), 7 (d) and 9 (e) wt% of SNP under 100x magnification using quadrant back scattering detector (QBSD)	131
Figure 4.32:	AFM topographic images of nanocomposite films of the P(3HB- <i>co</i> -44%4HB)/20 wt% chitosan cross-linked with	132

5% (w/v) of glutaraldehyde incorporated with 1 (a), 3 (b), 5 (c), 7 (d) and 9 (e) wt% of SNP and their three dimensional images (f, g, h, i & j)

- Figure 4.33: The degradation of the cross-linked P(3HB-*co*-44%4HB)/20 wt% chitosan blend film (A), nanocomposite films incorporated with 1 (B), 9 (C) wt% of SNP and P(3HB-*co*-44%4HB) (D) 147
- Figure 4.34 SEM images of the P(3HB-*co*-44%4HB) (a), cross-linked P(3HB-*co*-44%4HB)/20 wt% chitosan (b), nanocomposite films incorporated with 1 (c) and 9 (d) wt% of SNP before degradation and its images after degradation (e, f, g & h) 148

LIST OF APPENDICES

Appendix A: SEM images (1000 times of magnification)

Appendix B: Root mean square (RMS) images from AFM analysis

Appendix C: DSC thermograms

Appendix D: TGA thermograms

Appendix E: Images of clear zone (Disc diffusion method)

LIST OF SYMBOLS AND ABBREVIATIONS

Symbols and Abbreviations	Full Name
%	Percentage
μg	Microgram
μg/mL	Microgram per millilitre
μm	Micrometre
μL	Microlitre
θ	Theta
γ-BL	Gamma-butyrolactone
ω	Omega
α	Alpha
β	Beta
ΔH_m	Heat of fusion
2D	2 dimensional
3D	3 dimensional
3HB	3-hydroxybutyrate
3HB-CoA	3-hydroxybutyryl-CoA
4HB	4-hydroxybutyrate
4HB-CoA	4-hydroxybutyryl-CoA
3HV	3-hydroxyvalerate
AFM	Atomic force microscopy
Ag	Silver
ANOVA	Analysis of variance

ASTM	American Society for Testing and Materials
C	Carbon
$\text{CaCl}_2 \cdot 2\text{H}_2\text{O}$	Calcium chloride dihydrate
cal/g	Calorie per gram
CDW	Cell dry weight
CFU/mL	Colony forming units per millilitre
CLSI	Clinical and Laboratory Standards Institute
cm	Centimetre
CME	Caprylic methyl ester
CoA	Coenzyme-A
$\text{CoSO}_4 \cdot 7\text{H}_2\text{O}$	Cobalt (II) sulphate heptahydrate
CS	Chitosan
$\text{CuCl}_2 \cdot 2\text{H}_2\text{O}$	Copper (II) chloride dihydrate
Da	Dalton
DA	Degree of acetylation
dH ₂ O	Distilled water
DNA	Deoxyribonucleic acid
DSC	Differential scanning calorimeter
EDX	Energy dispersive X-ray
e-PHA	Extracellular-polyhydroxyalkanoate
fcc	Face centered cubic
FDA	Food and Drug Administration
$\text{FeSO}_4 \cdot 7\text{H}_2\text{O}$	Iron (II) sulphate heptahydrate

FTIR	Fourier transform infrared
g	Gram
GA	Glutaraldehyde
GC	Gas chromatography
g/L	Gram per litre
H	Hydrogen
HCl	Hydrogen chloride
H ₂ O	Water
H ₂ SO ₄	Sulphuric acid
ICI	Imperial Chemical Industries
IEC	Ionic exchange capacity
i-PHA	Intracellular-polyhydroxyalkanoate
IR	Infrared
IS	Internal standard
KCl	Potassium chloride
kDa	Kilodalton
KH ₂ PO ₄	Potassium dihydrogen phosphate
K ₂ HPO ₄	Dipotassium phosphate
kHz	kilohertz
L	Litre
LPS	Lipopolysaccharide
Ltd.	Limited
M	Molar
MBC	Minimum bactericidal concentration
mcl	Medium chain length

mg	Milligram
mg/mL	Milligram per millilitre
MgSO ₄ .7H ₂ O	Magnesium sulphate heptahydrate
MIC	Minimum inhibitory concentration
mL	Millilitre
mm	Millimetre
MM	Mineral medium
mmole/g	Millimole per gram
MnCl ₂ .4H ₂ O	Manganese chloride tetrahydrate
Mol%	Mole percent
MPa	Megapascal
mPEG	Monomethoxy poly(ethylene glycol)
M_w	Weight average molecular weight
N	Nitrogen
NA	Nutrient agar
NaCl	Sodium chloride
NADH	Nicotinamide adenine dinucleotide
NADPH	Nicotinamide adenine dinucleotide phosphate
Na ₂ HPO ₄	Disodium hydrogen phosphate
NaOH	Sodium hydroxide
Na ₂ SO ₄	Sodium sulphate
NH ₂	Amino
nm	Nanometre
NR	Nutrient rich

O	Oxygen
OD	Optical density
OH	Hydroxyl
P(3HB)	Poly(3-hydroxybutyrate)
P(4HB)	Poly(4-hydroxybutyrate)
P(3HB- <i>co</i> -3HHx)	Poly(3-hydroxybutyrate- <i>co</i> -3-hydroxyhexanoate)
P(3HB- <i>co</i> -4HB)	Poly(3-hydroxybutyrate- <i>co</i> -4-hydroxybutyrate)
P(3HB- <i>co</i> -3HV- <i>co</i> -4HB)	Poly(3-hydroxybutyrate- <i>co</i> -3-hydroxyvalerate- <i>co</i> -4-hydroxybutyrate)
PFRR	Polymers from renewable resources
PGA	Poly(glycolic acid)
PHA	Polyhydroxyalkanoate
PhaA; <i>phaA</i>	β -ketothiolase; gene encoding β -ketothiolase
PhaB; <i>phaB</i>	NADPH dependent acetoacetyl-CoA reductase; gene encoding NADPH dependent acetoacetyl-CoA reductase
PhaC; <i>phaC</i>	PHA synthase; gene encoding PHA synthase
<i>phaCAB</i>	three genes encoding PHA synthase, β -ketothiolase and NADPH dependent acetoacetyl-CoA reductase

PhaR; <i>phaR</i>	Repressor protein; gene encoding DNA-binding regulatory protein
PLA	Poly(L-lactic acid)
psi	Pounds per square inch
QBSD	Quadrant back scattering detector
R _a	Mean roughness
RMS	Root mean square
rpm	Rotational per minute
scl	Short chain length
SD	Standard deviation
SEM	Surface electron microscopy
SNP	Silver nanoparticle
sp.	Species
T _c	Crystallization temperature
T _d	Decomposition temperature
TDP	4,4'-thiodiphenol
TEC	Triethyl citrate
T _g	Glass transition temperature
TGA	Thermogravimetric analysis
T _m	Melting temperature
TMC	Trimesoyl chloride
UHMW-P(3HB)	Ultra high molecular weight-poly(3-hydroxybutyrate)
UV	Ultraviolet
v/v	Volume per volume

wt%	Dry weight percent
w/v	Weight per volume
w/w	Weight per weight
XRD	X-ray diffraction
ZnSO ₄ .7H ₂ O	Zinc sulphate heptahydrate

FABRIKASI DAN PENCIRIAN CAMPURAN POLI(3-HIDROKSIBUTIRAT- *ko*-4-HIDROKSIBUTIRAT)/KITOSAN DAN BAHAN NANOKOMPOSIT

PERAK

ABSTRAK

Pembalut luka yang ideal boleh mempercepatkan penyembuhan luka dengan mengawal jangkitan secara berkesan. Selain itu, terdapat beberapa kriteria pembalut luka yang penting seperti keupayaan menyerap cecair dari luka dan boleh dibiodegradasikan. Oleh itu, bahan campuran yang baru telah difabrikasi daripada poli(3-hidroksibutirat-*ko*-4-hidroksibutirat) [P(3HB-*ko*-4HB)] dan kitosan dengan menggunakan kaedah acuan pelarut yang mudah kerana polimer-polimer tersebut memenuhi ciri-ciri yang penting sebagai pembalut luka. Kesan kandungan kitosan (5, 10, 15 dan 20 b/b%) dan komposisi 4HB monomer (10, 18, 28 dan 44%) yang berbeza terhadap sifat filem hibrid telah dikenalpasti. Interaksi di antara P(3HB-*ko*-4HB) dan kitosan dalam bentuk ikatan hidrogen intermolekul telah disahkan melalui peralihan kumpulan karbonil kopolimer dan kumpulan amida kitosan pada spektrum FTIR. Kelarutan filem telah berkurang daripada 10% kepada 5% manakala kapasiti penyerapan air telah meningkat kepada 59-68% apabila kandungan kitosan adalah 20 b/b% di dalam setiap kopolimer. Selain itu, campuran dengan 20 b/b% kitosan telah meningkatkan pemanjangan pada takat putus dan menurunkan modulus Young kopolimer. Penurunan suhu lebur dan peningkatan kestabilan terma telah diperhatikan dari segi sifat terma. Imej mikroskopik menunjukkan filem campuran mempunyai permukaan yang berliang dan kasar. Di samping itu, filem tersebut mempamerkan perencatan yang baik terhadap *Escherichia coli* (22%) dan *Staphylococcus aureus* (11%). P(3HB-*ko*-4HB)/20 b/b% kitosan adalah lebih

hidrofilik, fleksibel, berliang, kasar dan mampu menghalang pertumbuhan bakteria. Oleh itu, filem campuran ini telah disilangkait secara kimia dengan kepekatan glutaraldehid yang berbeza [1, 3 dan 5% (b/i)]. Ikatan kovalen di dalam filem campuran yang telah disilangkait secara kimia disahkan melalui kehadiran jalur penyerapan di dalam lingkungan $1641-1631\text{cm}^{-1}$ yang mewakili ikatan imine. Di samping itu, ujian kapasiti pertukaran ion telah mendedahkan penyilangan di dalam filem campuran adalah setakat 52-55%. Kekuatan mekanikal filem campuran juga telah meningkat daripada 3 kepada 7 MPa. Walau bagaimanapun, keupayaan hidrofilik, kestabilan terma dan morfologi permukaan telah terjejas akibat kehadiran penyilangan di dalam matriks polimer. Prestasi antimikrob dengan jelas menunjukkan filem campuran telah mengurangkan pertumbuhan kedua-dua *E. coli* (35%) dan *S. aureus* (23%). P(3HB-ko-44%4HB)/20 b/b% kitosan yang telah disilangkait secara kimia dengan 5% (b/i) mempunyai tahap penyilangan yang tinggi berserta dengan kekuatan mekanikal, saiz liang dan kekasaran permukaan yang lebih baik dari filem lain. Oleh itu, aktiviti antimikrob filem tersebut dipertingkatkan dengan menggabungkan kandungan nanopartikel perak yang berbeza. Kehadiran nanopartikel perak telah disahkan melalui kajian FTIR dan XRD. Gabungan dengan nanopartikel perak telah meningkatkan kekuatan mekanikal, pemanjangan pada takat putus dan kekasaran permukaan. Pertumbuhan bakteria telah dihalang sehingga 100% oleh filem nanokomposit yang mengandungi nanopartikel perak sebanyak 9 b/b%. Akhir sekali, kajian degradasi dengan menggunakan lisozim mendedahkan filem campuran dan nanokomposit telah didegradasi dengan lebih cepat berbanding dengan kopolimer tulen disebabkan oleh kehadiran kitosan. Bahan-bahan bioaktif ini mempunyai masa depan yang cerah di dalam bidang pembalutan luka disebabkan oleh ciri-ciri fungsi mereka yang canggih.

FABRICATION AND CHARACTERIZATION OF POLY(3-HYDROXYBUTYRATE-co-4-HYDROXYBUTYRATE)/CHITOSAN BLEND AND ITS SILVER NANOCOMPOSITE MATERIAL

ABSTRACT

A desirable wound dressing should be able to accelerate wound healing with infection controlled effect. Other than that, there are few important features of the wound dressing such as ability to absorb the exudates from wound and to be biodegradable. Therefore, a new blend material was fabricated from poly(3-hydroxybutyrate-co-4-hydroxybutyrate) [P(3HB-co-4HB)] and chitosan through simple solvent casting method as they meet the essential requirements of the wound dressing. The impact of different contents of chitosan (5, 10, 15 and 20 wt%) and compositions of 4HB monomer (10, 18, 28 and 44%) towards the properties of hybrid film was determined. The interaction between P(3HB-co-4HB) and chitosan in the form of intermolecular hydrogen bonding was confirmed with the shift in the carbonyl group of copolymer and amide group of chitosan in the FTIR spectra. Film solubility was decreased from 10% to 5% whereas water absorption capacity was increased up to 59-68% when the content of chitosan was 20 wt% in each of the copolymer. Besides, blending with 20 wt% of chitosan improved the elongation at break and lowered the Young's modulus of the copolymers. In term of thermal properties, depression in the melting temperature and increment of thermal stability were observed. The microscopic images indicated that the blend films had porous and rough surface. Furthermore, they exhibited good inhibition against *Escherichia coli* (22%) and *Staphylococcus aureus* (11%). P(3HB-co-4HB)/20 wt% chitosan were more hydrophilic, flexible, porous, rougher and bactericidal. Therefore, these

blend films were chemically cross-linked via different concentrations of glutaraldehyde [1, 3 and 5% (w/v)]. The covalent bonding in the cross-linked blend films was confirmed with the presence of new absorbance band in a range of 1641-1631 cm^{-1} representing the imine linkage. Moreover, ionic exchange capacity test revealed the extent of cross-linking in the blend films was up to 52-55%. Interestingly, mechanical strength of the cross-linked blend films was also improved from 3 to 7 MPa. However, the hydrophilicity, thermal stability and surface morphology were adversely affected by the presence of cross-linking in the polymer matrix. The antimicrobial performance clearly showed that blend films greatly reduced the growth of both *E. coli* (35%) and *S. aureus* (23%). P(3HB-co-44%4HB)/20 wt% chitosan cross-linked with 5% (w/v) of glutaraldehyde had high degree of cross-linking together with good mechanical strength, pore size and surface roughness than other films. Therefore, the antimicrobial activity of this film was further enhanced by incorporating different contents of silver nanoparticle (SNP). The presence of SNP was verified by FTIR and XRD studies. Impregnation of SNP had resulted in improved mechanical strength, elongation at break and surface roughness. The bacterial growth was inhibited up to 100% by nanocomposite film with 9 wt% of SNP. Finally, degradation study using lysozyme revealed that the blend and nanocomposite films were degraded faster than the pure copolymer due to the presence of chitosan. These bioactive materials have a promising future in the wound dressing field due to their sophisticated functional properties.

1.0 INTRODUCTION

Recent advances in the science and technology enable mankind to invent and employ the new environmentally friendly materials instead of the synthetic based materials. Serious attention is paid in the innovation of these materials due to the increasing concern over the sustainability of our earth. Biodegradable polymers from renewable resources are the great alternative to resolve this issue because most of the countries are now reducing their plastic usage from the cheap fossil fuel; petroleum which will be depleted in future (Sudesh and Iwata, 2008). Based on the current dilemma, a benign approach such as development of greener polymeric materials without the usage of toxic or noxious component in their manufacturing process and the ability to degrade naturally is required (Ray and Bousmina, 2005).

Natural polymers have attractive properties such as non-toxicity, biodegradability and biocompatibility. Therefore, polymers have found diverse applications in biomedical field such as wound dressing. The main objective of the wound dressing is to accelerate the wound healing by providing optimum environment for wound repair with their functional properties. An ideal wound dressing should be able to absorb exudates from wound, elastic and resistance to microbe penetration to protect the wound from infection (Kokabi *et al.*, 2007). Despite of unique properties of polymers, the single homopolymer is unable to meet up the vast demand of a wound dressing, thus blending technique is selected to upgrade their performance (Kweon *et al.*, 2001). On the other hand, blending the natural polymers is very challenging since the natural polymers have irregular molecular structures such as wide range of molecular masses. Therefore, controlling the processing factors is crucial as these decisive factors have huge effect in developing a reproducible product (Moraes *et al.*, 2010).

Polyhydroxyalkanoate (PHA) is synthesized by microbes under the stress condition when phosphorus or nitrogen is limited and in the presence of excessive carbon supply. This stage is known as accumulation stage whereby the cells will not divide or grow but they will convert their metabolism towards biosynthesis (Jurasek and Marchessault, 2004). Poly(3-hydroxybutyrate) [P(3HB)] and their copolymers are the mostly known members of PHA (Noda *et al.*, 2005).

Poly(3-hydroxybutyrate-*co*-4-hydroxybutyrate) [P(3HB-*co*-4HB)] copolymer can be tailored into different monomer compositions by the utilization of different carbon sources for the 3HB and 4HB monomers generation (Lee *et al.*, 2004). In fact, general precursors namely 4-hydroxybutyrate, γ -butyrolactone and 1,4-butanediol have the ability to produce the P(3HB-*co*-4HB) (Valentin and Dennis, 1997). Besides, the properties of the copolymer can be altered from hard crystalline plastics to very elastic rubber through the manipulation of the 4HB content (Martin and Williams, 2003). However, P(3HB-*co*-4HB) has a few drawbacks in the properties such as absence of hydrophilicity and bioactivity. Therefore, blending with another polymer should be done in order a new low cost product can be obtained with diverse properties (Keshavarz and Roy, 2010).

Moreover, blending with natural polymer such as polysaccharides is an excellent way to develop a novel biomaterial because they have active groups such as amine, amide and hydroxyl which will enable the interaction with PHA macromolecules (Moraes *et al.*, 2010). Chitosan is one of the natural polysaccharide obtained from the removal of *N*-acetyl group of chitin and it is a linear copolymer linked by β -1,4 glycosidic bonds (Wu, 2005; Yap *et al.*, 2011). Chitosan has gained interest due to its filmogenic property, antimicrobial activity, biocompatibility, biodegradability, non-toxic and of low cost (Camacho *et al.*, 2010; Witt *et al.*, 2010).

These characteristics of chitosan opened the window for the pharmaceutical and biomedical applications (Ramachandran *et al.*, 2011).

Nanoparticle in a scale of 1-100 nm has larger surface area and surface atoms than the microscale sized particles (Azeredo, 2009). As one of the member, silver nanoparticle (SNP) has created a new era in overcoming the resistance of bacteria against antibiotics (Vimala *et al.*, 2010). The antimicrobial efficiency of the developed blend film can be upgraded by incorporating this nanoparticle into the polymer matrix. As a result, a novel nanocomposite of P(3HB-*co*-4HB), chitosan and SNP can be fabricated.

This work aims to shed light in the fabrication of blend film and nanocomposite material as wound dressing. The attempt of this study is to develop a biomaterial based on the following components namely P(3HB-*co*-4HB), chitosan and SNP which will be investigated thoroughly in term of their physical, chemical, thermal and biological properties. Two different approaches will be applied in the blending of the polymers such as simple solvent casting technique and chemical cross-linking via glutaraldehyde. One of the methods will be selected based on the properties and SNP will be incorporated into the polymeric matrix to create a nanocomposite with improved antimicrobial performance. Finally, the *in vitro* degradation of the blend and nanocomposite films using lysozyme will be carried out.

Thus, there are several objectives that need to be achieved at the end of this research:

- 1) To fabricate P(3HB-*co*-4HB)/chitosan blend films with hydrophilic and antimicrobial property in different formulations by varying the composition of P(3HB-*co*-4HB) and content of chitosan.
- 2) To study the effect of fabrication techniques on the physical, chemical, thermal and biological properties of the blend material.
- 3) To enhance the antimicrobial activity of the blend film by the incorporation of the SNP and to investigate the *in vitro* biodegradability of the blend and nanocomposite films.

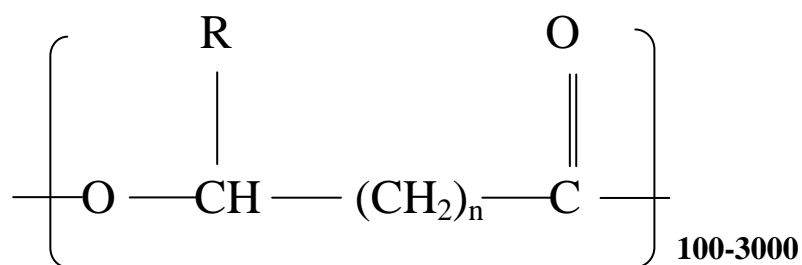
2.0 LITERATURE REVIEW

2.1 Polyhydroxyalkanoate (PHA)

Polyhydroxyalkanoate (PHA) is the polymer of hydroxyalkanoate that is intracellularly synthesized as distinct granule when the growth is limited whereas the carbon source should be in excessive form (Choi and Lee, 1999). All the PHAs share similar characteristics among themselves such as hydrophobicity (insoluble in water), high degree of polymerization ($10^5 - 10^7$ Da), non-toxicity, biocompatibility, inherent biodegradability and they are enantiomerically pure chemicals consisting only *R*-stereoisomer (Steinbüchel, 2001).

PHA is classified into two categories namely short chain length PHA (*scl*-PHA) and medium chain length PHA (*mcl*-PHA) consisting of 3-5 carbon atoms and 6-16 carbon atoms, respectively (Akaraonye *et al.*, 2010). The material properties can be identified based on the component monomer as the *scl*-PHA is thermoplastic and can be very brittle whereas the *mcl*-PHA is elastomeric and become softer when the monomeric chain length increases (Thomson *et al.*, 2010).

P(3HB) homopolymer is an eminent member of the PHA and its copolymers are synthesized by the incorporation of secondary monomer (*scl*-PHA) such as 3-hydroxyvalerate (3HV) and 4-hydroxybutyrate (4HB) (Taguchi and Doi, 2004). Moreover, copolymer consisting of *scl*-PHA and *mcl*-PHA such as poly(3-hydroxybutyrate-*co*-3-hydroxyhexanoate) [P(3HB-*co*-3HHx)] can also be synthesized (Nomura *et al.*, 2004). In addition, copolymerization of different monomers leads to the formation of terpolymer such as poly(3-hydroxybutyrate-*co*-3-hydroxyvalerate-*co*-4-hydroxybutyrate) [P(3HB-*co*-3HV-*co*-4HB)] (Amirul *et al.*, 2008a). The common structure of the PHA is shown in Figure 2.1.



n=1	R=hydrogen	poly(3-hydroxypropionate)	P(3HP)
	R=methyl	poly(3-hydroxybutyrate)	P(3HB)
	R=ethyl	poly(3-hydroxyvalerate)	P(3HV)
	R=propyl	poly(3-hydroxycaproate)	P(3HC)
	R=butyl	poly(3-hydroxyheptanoate)	P(3HH)
	R=pentyl	poly(3-hydroxyoctanoate)	P(3HO)
	R=hexyl	poly(3-hydroxynonanoate)	P(3HN)
	R=heptyl	poly(3-hydroxydecanoate)	P(3HD)
	R=octyl	poly(3-hydroxyundecanoate)	P(3HUD)
	R=nonyl	poly(3-hydroxydodecanoate)	P(3HDD)
n=2	R=hydrogen	poly(4-hydroxybutyrate)	P(4HB)
n=3	R=hydrogen	poly(5-hydroxyvalerate)	P(5HV)

Figure 2.1: Chemical structure of the PHA (Wu *et al.*, 2003).

There are about 150 different constituents of PHA and the biosynthesis of these PHAs occurs due to the broad substrate ranges of the PHA synthase. Based on the composition of the subunit (PhaC, PhaC with PhaE or PhaR) and substrate specificity of the PHA synthase, it is classified into different classes namely class I, class II, class III and class IV (Steinbüchel and Eversloh, 2003). PHA synthase is the last enzyme involved in the biosynthesis of PHA whereby it was found in soluble form during normal growth condition and transformed into granule associated under nitrogen limiting condition (Müller and Seebach, 1993).

The PHA synthesis will not take place in the presence of PHA synthase alone because there are other enzymes present in the system such as β -ketothiolase and NADPH-dependent acetoacetyl-CoA reductase. Three genes that are located in one operon (*phaCAB* operon) in *Ralstonia eutropha* are responsible for the encoding of these enzymes. *phaA*, *phaB* and *phaC* are required for the formation of β -ketothiolase, NADPH-dependent acetoacetyl-CoA reductase and PHA synthase, respectively (Grage *et al.*, 2009).

There are two types of depolymerase enzyme in the PHA degradation system such as intracellular (i-PHA) and extracellular (e-PHA) depolymerase enzyme (Contreras *et al.*, 2012). Biodegradability of the PHA in natural environment is due to the extracellular degrading enzyme namely PHA depolymerase that hydrolyzes the solid high molecular weight polymer into water soluble monomer and oligomers. Microorganisms such as bacteria and fungi secrete this enzyme as PHA is unable to move across the cell wall because of its high molecular weight. Finally, the degraded products will move through the cell wall and become metabolized (Numata *et al.*, 2009).

2.1.1 Poly(3-hydroxybutyrate) [P(3HB)]

The first discovered PHA is poly[(*R*)-3-hydroxybutyrate] [P(3HB)], a linear homopolymer consisting of (*R*)-3-hydroxybutyric acid units which are linked together through ester bonds between the 3-hydroxyl group and the carboxyl group of the following monomer (Müller and Seebach, 1993 & Zinn *et al.*, 2001). There are various P(3HB) producers but only few have been employed to synthesize P(3HB) namely *Cupriavidus necator* (previously known as *Ralstonia eutropha*) (Fukui *et al.*, 2009), *Alcaligenus latus* (Wang *et al.*, 2013) and *Azotobacter vinelandii* (Reddy and Mohan, 2012).

P(3HB) homopolymer is known to be a semicrystalline polymer exhibiting high crystallinity and melting point (T_m) around 180°C. It becomes thermally unstable when the decomposition temperature is very near to the T_m during the melt processing (Pan and Inoue, 2009). Furthermore, the properties of this homopolymer change from one sample to another according to certain criteria such as production organism, extraction techniques and sample preparation methods. Despite of this, low molecular weight P(3HB) presents naturally in human blood and degrades into 3-hydroxybutyric acid indicating its remarkable biocompatibility and non-toxicity (Misra *et al.*, 2006).

P(3HB) has a weight-average molecular weight (M_w) in a range of 5×10^5 – 10×10^5 Da. The molecular weight of the P(3HB) also limits its application in hot drawing since it undergoes fast thermal degradation when the processing temperature is close to its melting point (Kahar *et al.*, 2005). Therefore, ultra-high-molecular-weight P(3HB) [UHMW-P(3HB)] is synthesized by recombinant *Escherichia coli* which can be subjected to the hot drawing procedure (Kusaka *et al.*, 1997).

The synthesis of P(3HB) starts with the condensation of two acetyl-CoA molecules to form acetoacetyl-CoA catalyzed by β -ketothiolase. The product is reduced into (*R*)-3-hydroxybutyryl-CoA by NADPH dependent acetoacetyl-CoA reductase. The latter will be linked to the expanding chain of P(3HB) polyester by PHA synthase (Rehm, 2006). In this biosynthesis pathway, two enzymes namely thiolase and reductase supply the monomers required for the polymerization reaction. Therefore, the kinetic characteristics and substrate specificities of these enzymes are important in the resulting compounds (Madison and Huisman, 1999). Moreover, NADH and NADPH concentrations also play a crucial role in the biosynthesis pathway (Figure 2.2) as they will inhibit the citrate synthase to enable the metabolic flux of acetyl-CoA into the pathway (Kessler and Witholt, 2001).

The intracellular concentration of P(3HB) can be detected through the recovery of the polymer from chloroform or via gas chromatography. Recovery of polymer from the cells occurs in a stepwise procedure starting from freeze drying the cells and followed by extraction in hot chloroform using the Soxhlet extractor. The purity of the polymer is ensured by washing the polymer twice with methanol and vacuum dried (Tokiwa and Ugwu, 2007). Direct quantification of P(3HB) is carried out with the acid methanolysis of the cells before the gas chromatography analysis (Braunegg *et al.*, 1978).

Degradation of polymers can take place via microbes or by enzymes. In term of microbial degradation, there is a wide range of organisms at ambient or mesophilic and few at higher temperature which are capable for the degradation. The enzymatic degradation is known as a hydrolysis reaction whereby the enzyme will bind on the surface of polymer followed by the hydrolytic cleavage (Tokiwa and Calabria, 2004).

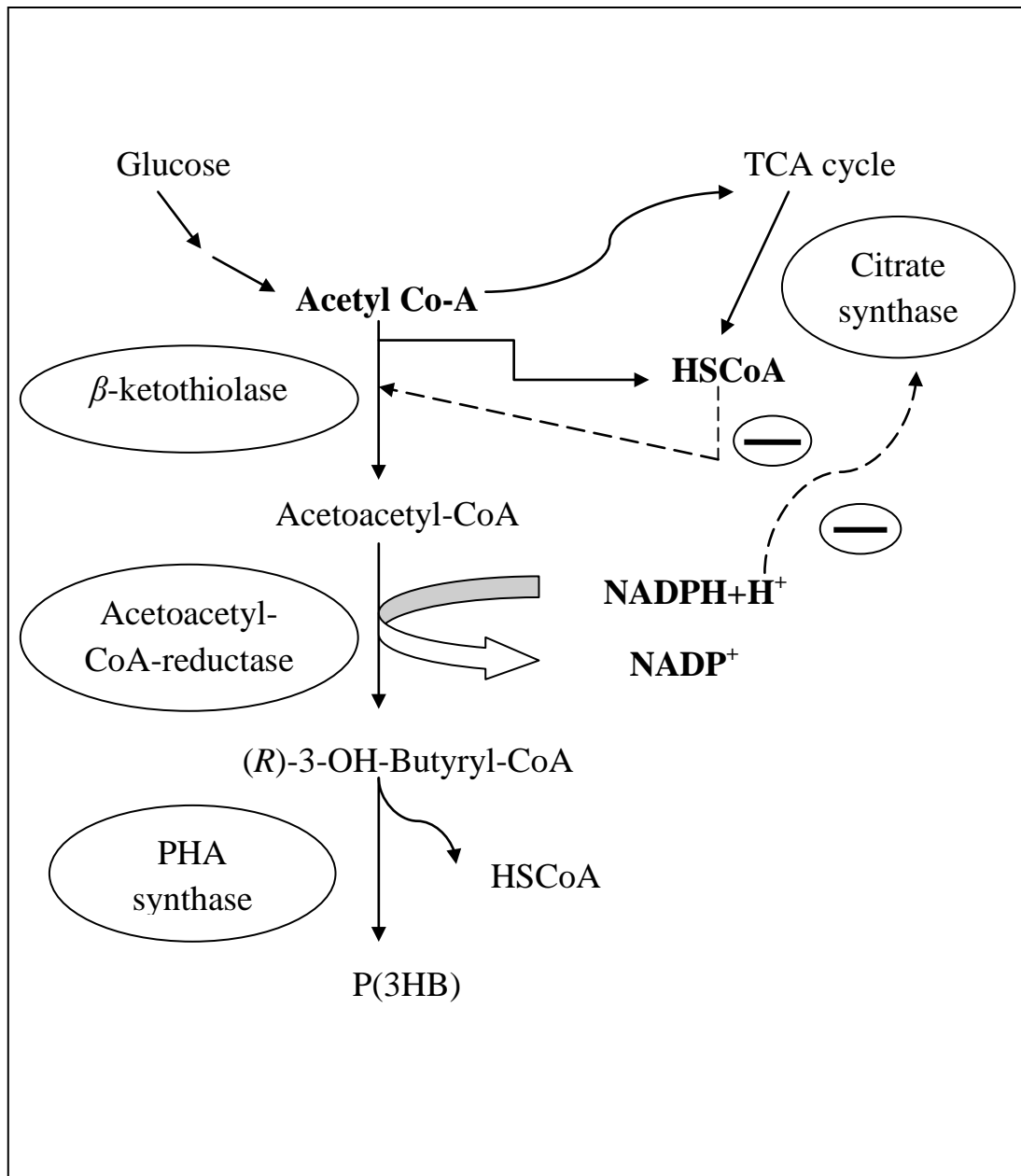


Figure 2.2: The three step biosynthesis pathway of P(3HB). Hatched arrows indicate the negative regulatory effects whereas the critical metabolites and cofactors are written in bold (Kessler and Witholt, 2001).

2.1.2 Poly(4-hydroxybutyrate) [P(4HB)]

Poly(4-hydroxybutyrate) [P(4HB)] homopolymer originates from a diverse class of material known as PHA. There are three wild type bacteria producing P(4HB); *Cupriavidus necator* (Kimura *et al.*, 1999), *Comamonas acidovorans* (Sudesh *et al.*, 1999) and *Hydrogenophaga pseudoflava* (Choi *et al.*, 1999). P(4HB) has a similar chemical structure with the absorbable polyesters which are utilized as implantable medical products. Therefore, P(4HB) has gained its interest in many medical applications namely cardiovascular, wound healing, orthopedic, drug delivery and tissue engineering. Moreover, P(4HB) is preferably produced from fermentation rather than chemical synthesis which resulted in low molecular weight polymer that is unfavourable for most of the applications (Martin and Williams, 2003).

Therefore, Tepha Inc. (Cambridge, MA) is a medical device company which commercially produces P(4HB) via transgenic fermentation process by using recombinant *Escherichia coli* K12 and markets it for medical purposes (Martin and Williams, 2003). P(4HB) homopolymer is strong and flexible thermoplastic when compared with the synthetic polymers and it has high tensile strength (Philip *et al.*, 2007). P(4HB) exhibits glass transition temperature (T_g) at around -50°C and melting temperature at around 60°C based on the calorimetric analysis (Kim *et al.*, 2006).

The final degradation products of the ester linkages of P(4HB) by hydrolysis are γ -butyrolactone (γ -BL) and 4-hydroxybutyric acid (4HB) which are generally the same *in vivo* as the γ -BL undergoes a rapid ring opening catalysed by the enzyme γ -lactonase yielding 4HB in the body (Moore *et al.*, 2005). Moreover, 4HB is a natural human metabolite exists in the organs such as brain, lung, heart, liver, kidney and muscle (Nelson *et al.*, 1981). The latter is very quickly absorbed to peak

concentration of 4HB in 20 to 45 minutes and metabolized by succinic acid semialdehyde to succinic acid with an elimination half-life of 30 to 50 minutes (Ferrara *et al.*, 1992).

Based on good understanding about the pharmacology of P(4HB), Food and Drug Administration (FDA) allowed the usage of large doses of this metabolite to treat the patients with narcolepsy. On the other hand, small P(4HB) implants will not cause any pharmacological effects due to the slow conversion of P(4HB) to 4HB followed by rapid metabolism of 4HB (Martin and Williams, 2003).

P(4HB) has an added advantage in the medical field when compared with the synthetic polymers namely poly(L-lactid acid) [PLA] and poly(glycolic acid) [PGA] since their degradation products may lead to inflammatory reaction due to the acidity of the end products. On the other hand, P(4HB) exhibits good mechanical properties and less *in vivo* tissue reaction (Valappil *et al.*, 2006). It is apparent that P(4HB) can be distinguished from other synthetic polymer namely PGA based on mechanical and thermal properties as well as mechanism of degradation (Table 2.1).

Table 2.1: The general differences between P(4HB) and PGA (Martin and Williams, 2003).

Properties	P(4HB)	PGA
Thermal property	Low melting temperature	High melting temperature
Tensile strength	Strong	Very strong
Tensile modulus	Flexible	Stiff
Ability to elongate	High	Virtually none
Absorption rate	Moderate	Very fast
Loss of strength <i>in vivo</i>	Gradual loss	Rapid
Degradation products	Less acidic	Highly acidic
Inflammatory reaction	Well tolerated	Can be severe
Thermoplastic melt processing	Yes	Yes
Solvent processing	Soluble in range of solvents	Virtually insoluble
Resistant to moisture	Fairly good	Poor

2.1.3 Poly(3-hydroxybutyrate-co-4-hydroxybutyrate) [P(3HB-co-4HB)]

Poly(3-hydroxybutyrate-co-4-hydroxybutyrate) [P(3HB-co-4HB)] copolymer is known as a good biomaterial due to the presence of the 4HB monomer which is able to reduce the polymer crystallinity (Chanprateep *et al.*, 2010). The properties of this copolymer (Table 2.2) can be tailored by the incorporation or alteration of the comonomer composition since high 4HB content able to defect the matrix of crystal lattice resulting in lower melting temperature (T_m), glass transition temperature (T_g) and enthalpy of fusion (ΔH_m) (Cong *et al.*, 2008b). Besides, P(4HB) is a highly ductile, flexible polymer with extension to break up to 1000% whereas P(3HB) only exhibits 10% of extension to break. Therefore, incorporation of 4HB improves the flexibility and toughness of the polymer (Valappil *et al.*, 2006).

P(3HB-co-4HB) is produced by using different carbon precursors such as γ -butyrolactone, 1,4-butanediol, 1,6-hexanediol, 1,8-octanediol, 1,10-decanediol and 1,12-dodecanediol. Generally, the composition of the copolymer is manipulated by using different combinations of precursors or by varying the concentration of the precursors (Amirul *et al.*, 2008a; Vigneswari *et al.*, 2009). Up to now, there are five wild producers of this copolymer namely *Alcaligenes latus* (Kang *et al.*, 1995), *Comamonas testosteroneii* (Renner *et al.*, 1996) *Hydrogenophaga pseudoflava* (Choi *et al.*, 1999) *Comamonas acidovorans* (Lee *et al.*, 2004) and *Cupriavidus necator* (Kim *et al.*, 2005). Apart from this, *Cupriavidus necator* has been studied extensively and able to synthesize P(3HB-co-4HB) copolymer with different 4HB fractions (0-100 mol%) (Kim *et al.*, 2005). There are *Cupriavidus* strains isolated from Malaysian environment which are capable to produce this copolymer namely *Cupriavidus* sp. USMAA1020, *Cupriavidus* sp. USMAA2-4 and *Cupriavidus* sp. USMAHM13 (Rahayu *et al.*, 2008; Amirul *et al.*, 2008b & Ramachandran and

Table 2.2: Thermal properties of different compositions of P(3HB-co-4HB) copolymer (Nakamura and Doi, 1992).

Monomer composition (mol%)		Melting point (°C) (T_m)	Glass transition temperature (°C) (T_g)	ΔH_m (cal/g)	Crystallinity (%)
3HB	4HB				
100	0	177	4	20.8	59 ± 5
94	6	162	-1	13.5	56 ± 5
90	10	159	-3	13.0	46 ± 5
72	28	0	-15	-	23 ± 5
15	85	48	-41	8.6	29 ± 5
10	90	50	-44	10.2	-
6	94	51	-46	11.0	42 ± 5
0	100	54	-50	11.0	-

Amirul, 2013).

In the synthesis pathway of P(3HB-*co*-4HB), the carbon precursors are generally converted into 4HB. As for γ -butyrolactone, it is hydrolytically cleaved into 4HB by esterases or lactonases and metabolized into 4-hydroxybutyryl-CoA (4HB-CoA). In case of ω -alkanediols, they are oxidized via two enzymatic reactions, one directly into 4HB and another is first oxidized into ω -hydroxyfatty acids which are converted to coenzyme A thioester. The latter is subjected into β -oxidation for the formation of 4HB-CoA. Later, the 4HB-CoA is polymerized by PHA synthase as in Figure 2.3 (Steinbüchel and Eversloh, 2003).

P(3HB-*co*-4HB) stands a good chance in the biomedical applications as the 4HB is a natural human metabolite (Nelson *et al.*, 1981). This is because P(3HB-*co*-4HB) has the ability to be hydrolyzed by eukaryotic lipases into natural metabolites similar to those present in human body (Doi *et al.*, 1990). All these prove that P(3HB-*co*-4HB) copolymer has a great future in medical and pharmaceutical applications due to its attractive features (Bach *et al.*, 2009). P(3HB-*co*-4HB) copolymer is commonly degraded by two enzymes namely PHA depolymerase and lipase. The rate of enzymatic reaction against P(3HB-*co*-4HB) increases with higher 4HB fraction when compared with P(3HB) homopolymer (Kang *et al.*, 1995). However, the rate of degradation of P(3HB-*co*-4HB) with high molar fraction of 4HB decreases when PHA depolymerase is used since P(4HB) sequences tend to crystallize. However, lipase degrades 4HB monomer instead of 3HB monomer and the degradation rate increases with the content of 4HB. (Mitomo *et al.*, 2001). Apart from that, lysozyme might also able to accelerate *in vivo* degradation of P(3HB) (Zhijiang *et al.*, 2012). Normally, lysozyme was secreted by the body's immune system to catalyze the degradation of the P(3HB) (Sultana and Khan, 2012).

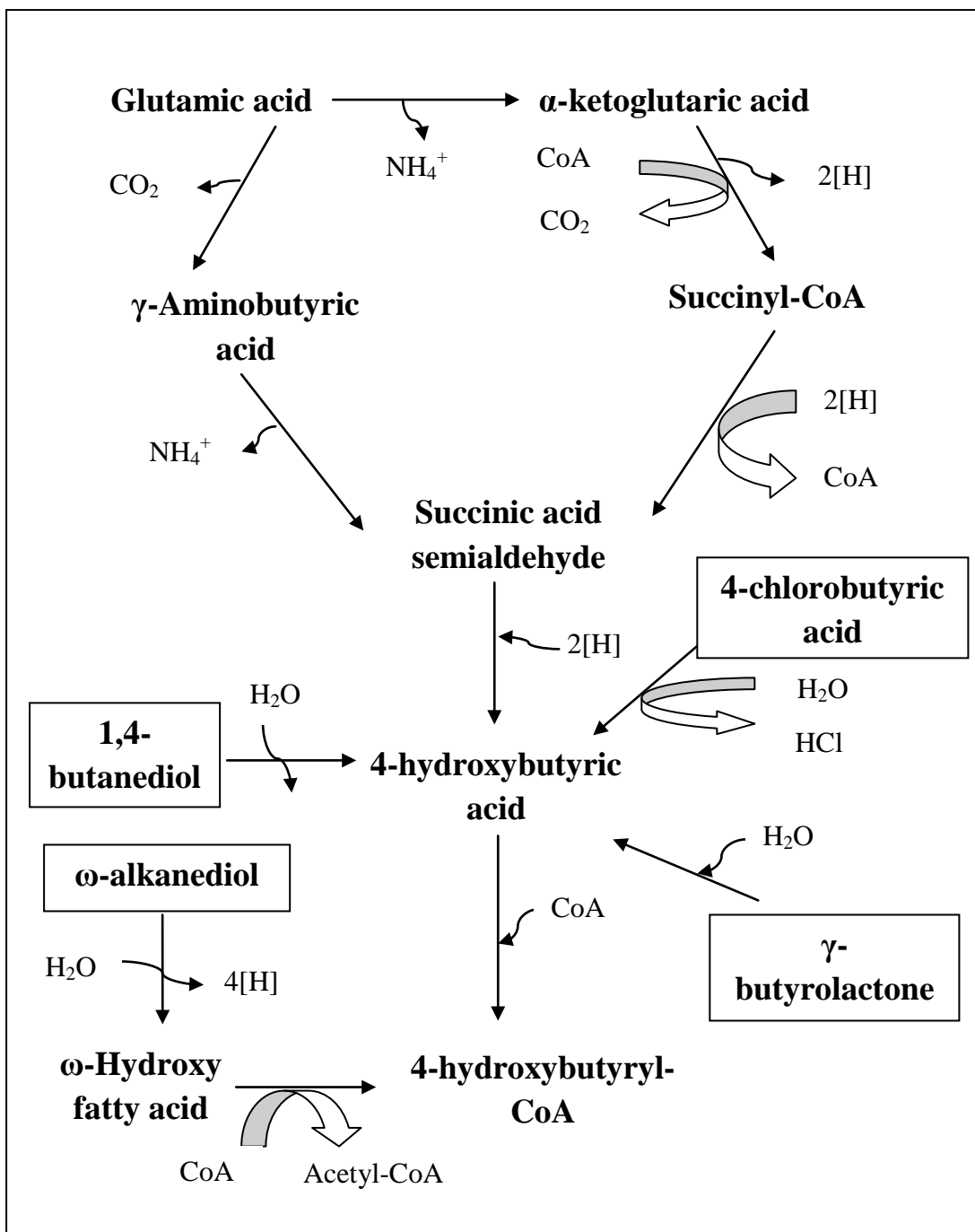


Figure 2.3: Biosynthesis pathway of P(3HB-co-4HB) from different carbon precursors (Steinbüchel and Eversloh, 2003).

2.2 Chitosan (CS)

Chitosan is derived from deacetylation of chitin under alkaline condition. The degree of deacetylation (DA) of the resulting CS can be up to 0.95 and complete deacetylation is achieved by repeating the process. Generally, the DA is determined by infrared (IR) spectroscopy via the absorption ratios (Honarkar and Barikani, 2009). DA of CS will determine its physicochemical properties namely molecular weight and mechanical properties. It also affects the biological properties such as biodegradation by lysozyme, wound healing and osteogenesis enhancement (Dhiman *et al.*, 2004).

CS consists of 2-acetamido-2-deoxy- β -D-glucopyranose and 2-amino-2-deoxy- β -D-glucopyranose residues and it is found by Professor C. Rouget in 1859 (Bhatnagar and Sillanpää, 2009). The backbone of CS is very similar with cellulose containing β -1,4-linked-D-glucosamine with different degrees of N-acetylation. However, in CS, acetylamino group replaces the hydroxyl group in the C2 position of the cellulose (Figure 2.4). CS is a natural polymer whereas chitin is the second abundant polymer which is present in the exoskeleton of crustaceans, fungi and insects (Dash *et al.*, 2011).

CS has commercial importance because of the higher percentage of nitrogen than the synthetically substituted cellulose. CS is a good functional material because it has many desirable characteristics namely biodegradability, biocompatibility, adsorption and non-toxicity (Kumar, 2000). In term of biodegradability, lysozyme is able to degrade the chitosan due to the presence of *N*-acetylglucosamine (Honma *et al.*, 2006). Its biocompatibility has a crucial part in biomedical domain and materials prepared from CS namely sponges, films, hydrogels and fibers are useful in medical

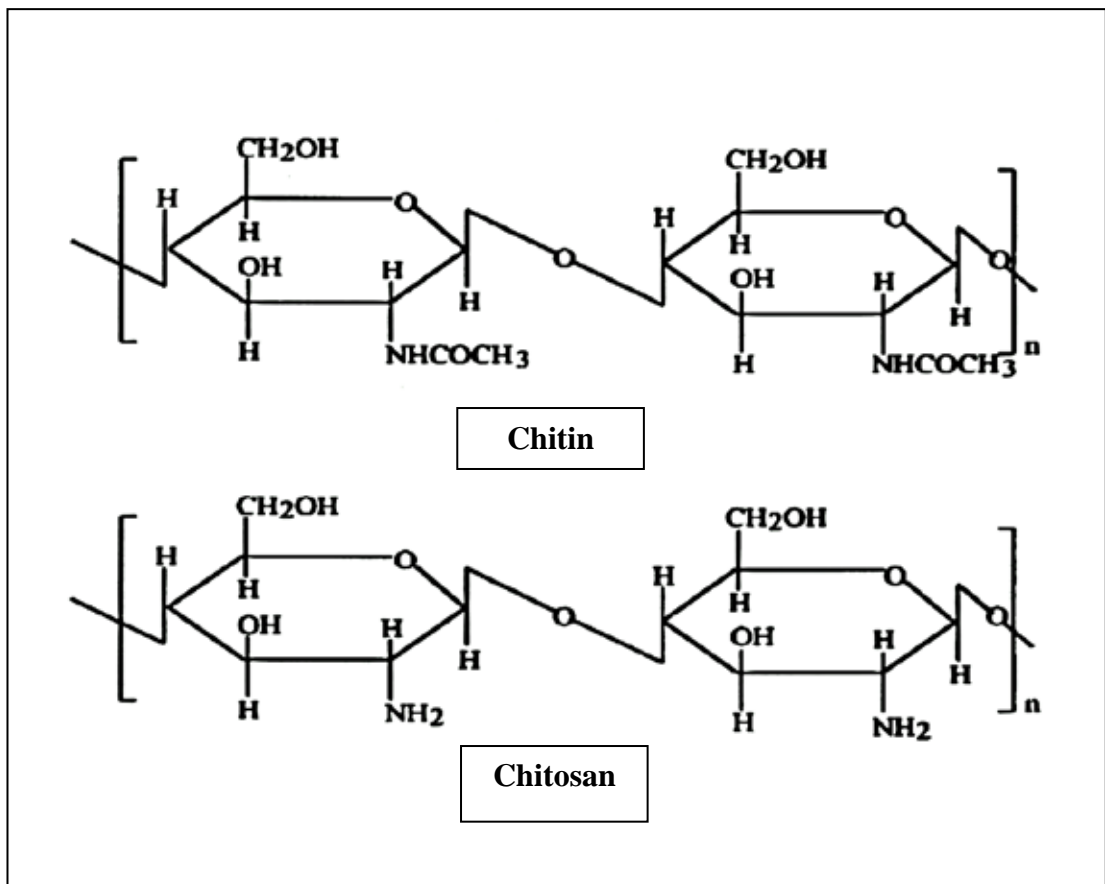


Figure 2.4: Structure of chitin and chitosan (Kumar, 2000).

applications. Another advantage of CS is hydrophilicity which is due to its polar groups (OH and NH₂) that enable it to form secondary interactions (Rinaudo, 2006).

Antimicrobial activity of CS has received great attention due to the consistent problems regarding the synthetic chemical agents. The antimicrobial activity arises from the cationic charge of CS and enables it to aggressively bind onto the microbial cell surface causing membrane shrinkage and finally death of the cell (Prashanth and Tharanathan, 2007). The antimicrobial activity differs accordingly with the category of CS mainly degree of deacetylation, target organisms, molecular weight and conditions of the medium such as pH, presence of solutes and ionic strength that are suitable to interact with CS via covalent binding or electrostatic interaction that can inhibit the antimicrobial activity (Aider, 2010). CS has a broad spectrum of antimicrobial activity and the mechanisms vary among Gram-negative, Gram-positive bacteria and fungi due to the cell surface characteristics of these organisms (Kong *et al.*, 2010).

CS possesses the ability to accelerate the wound healing process by promoting rapid dermal regeneration (Shi *et al.*, 2006). Therefore, CS stands a good chance to be applied as a biological dressing (bioactive dressing) (Boateng *et al.*, 2008). Nowadays, CS is utilized as a wound dressing in burn healing for the proliferation and activation of inflammatory cells in granulation tissue and to accelerate the wound cleaning and re-epithelisation (Alemdaroglu *et al.*, 2006; Ueno *et al.*, 2001). CS administration also seems to increase the supply of oxygen and vitamin C resulting in the progression of the wound healing (Ueno *et al.*, 1999). The wounds close up in 14 days and the mature epidermal architecture is found with keratinized surface of normal thickness and a subsided inflammation in the dermis (Dash *et al.*, 2011).

2.3 Blending polymers from renewable resources (PFRR)

Polymers from renewable resources (PFRR) are divided into three categories; natural polymers namely starch, cellulose, chitosan and protein, synthetic polymers from natural monomers namely polylactide acid (PLA) and polymers synthesized by microbes namely polyhydroxyalkanoate (PHA) which is shown in Figure 2.5. The performance of these PFRR is enhanced and altered via blending and composite formation (Yu *et al.*, 2006). There are various numbers of polymers that can be combined to form blend with different physical properties. The characteristics of the polymeric blend are influenced by the nature of the dispersed and dispersion phases, the volume ratio of the phases, the sizes and size distributions of the particles of the dispersed phase and interfacial adhesion (Prut and Zelenetskii, 2001).

Polymer blending has gained researchers focus because polymer with extraordinary properties obtained by chemical synthesis is more expensive than the existing polymers and blending operation. Furthermore, a wise choice and combination of the polymeric materials in specific amount may lead to fabrication of blend material with the desired properties. One of the popular questions being addressed regarding the polymer blend is the miscibility between the components. It can be miscible, partially miscible or fully immiscible. The miscible polymer blend is formed by choosing polymers with a compatible chemical structure which are capable of specific interaction (Utracki, 2002).

There are different types of polymer blends such as simple binary mixtures, combination of block copolymers and homopolymers, interpenetrating networks, reactive compatibilized systems, molecular composites, impact modified polymers, emulsion blends, engineering polymer blends and so on. The properties of the blend are dependent on the method of preparation that is employed to prepare the blend. It

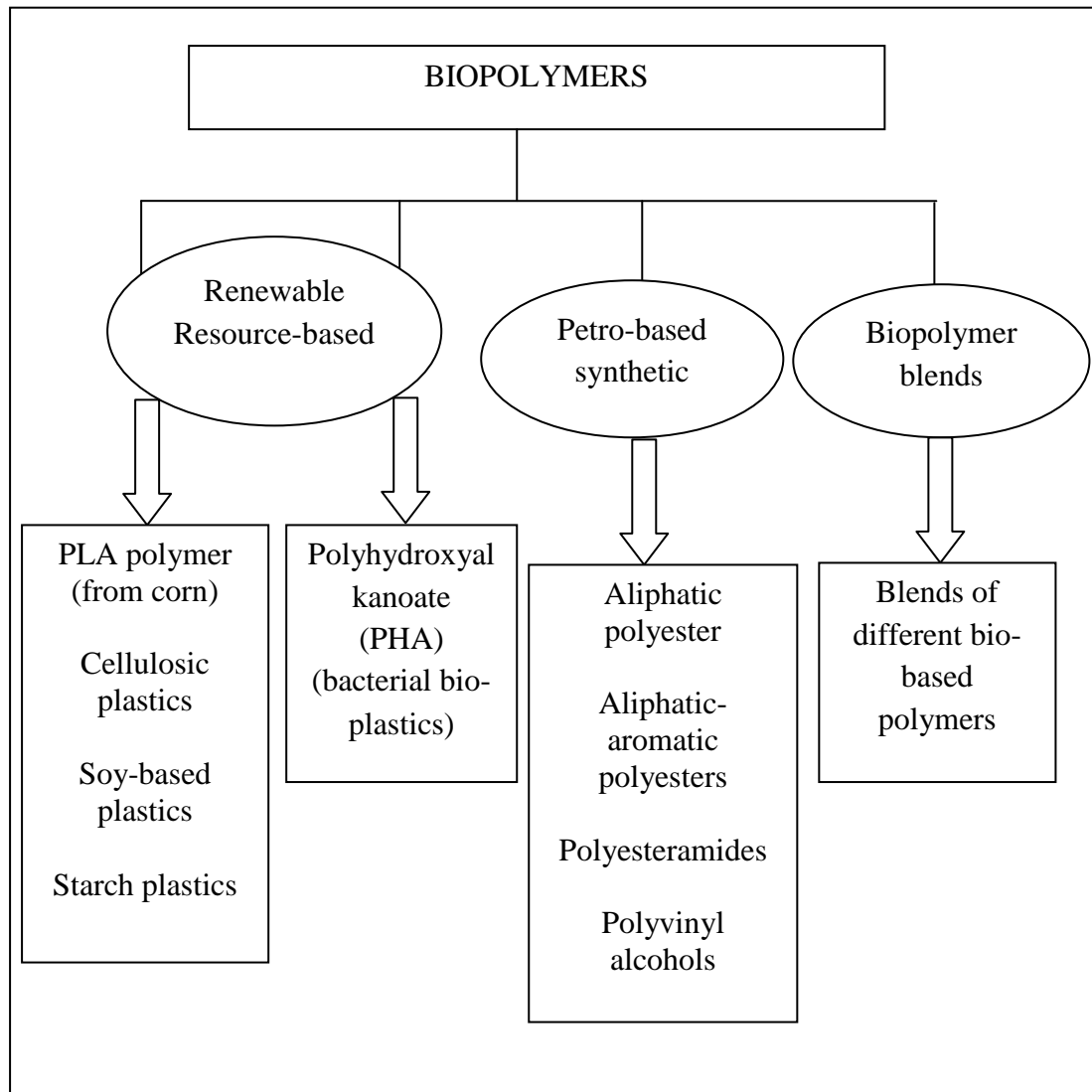


Figure 2.5: Classification of the biopolymers from three different sources (Mohanty *et al.*, 2002).

can be as simple as mixing the polymer powders with heating or it can be performed via solvent mixing, mechanical mixing including high shear intensity mixing and *in situ* polymerization which may or may not yield a covalent bonding (Robeson, 2007).

2.3.1 Solution blending

Solution blending method is the most favourable method used in a laboratory scale whereby the blend components are dissolved in a common solvent or different solvents followed by intensive stirring. The blend is fabricated by evaporation or precipitation of the solvent. The formation of the phase structure depends on the blend composition, interaction parameter of the blend components and type of solvent. The advantage of this technique will be its rapid mixing of the components without the unfavourable chemical reactions (Wiley & Sons, 2011).

In this physical method, the handling of the small quantity of the experimental polymer is easier and degradation problem is not encountered. The disadvantage of this method is not all the polymers can dissolve in the same solvent. Furthermore, residual solvent can affect the analysis of the blend film. The rate of evaporation is a crucial element in morphology and miscibility of the blend as the removal of the diluents may lead to uncertain changes to the phase morphology which weakens the blend (Boudenne *et al.*, 2011).

2.3.2 Modification of polymer blend via cross-linking

Polymer modification (Figure 2.6) can also be performed via chemical cross-linking that is also known as covalent cross-linking. This is a mechanism related with covalent bonding between the chains of the polymer by chemical reaction which forms a certain number of tie or junction points (Song *et al.*, 1999). Chemical cross-linking is a direct technique in creating a permanent network and it is formed by small molecule cross-linkers, polymer-polymer reactions between activated functional groups and photosensitive agents or enzyme catalysed reactions (Bhattarai *et al.*, 2010).

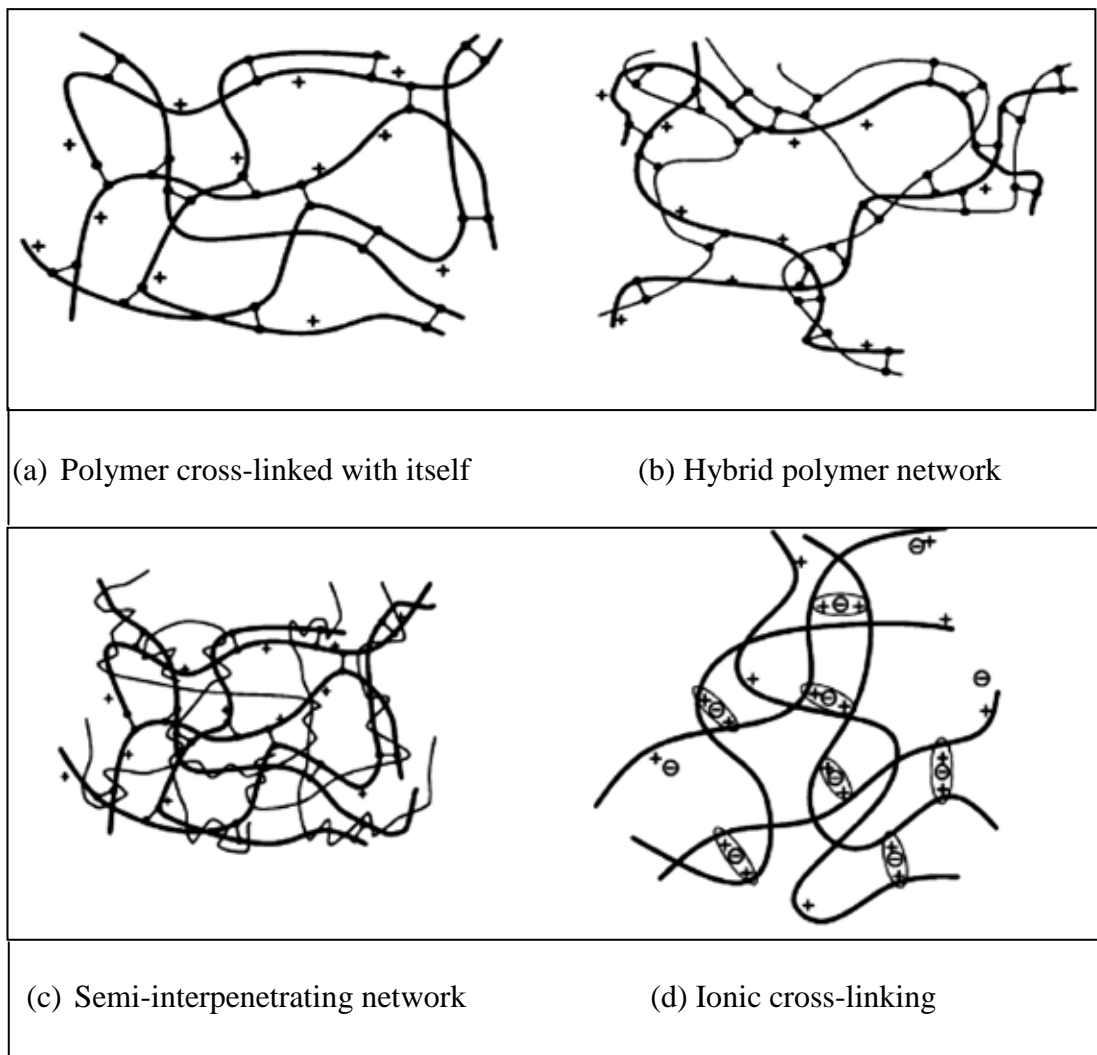


Figure 2.6: Structure of polymer network (●—● , covalent cross-linker; +, positive charge of polymer; —, polymer; —, additional polymer; ⊕, charged ionic cross-linker; ⊖, ionic interaction (Berger *et al.*, 2004).

Cross-linking prevents the chain from gliding past one another and produces elasticity in an amorphous polymer. It causes the blend to be resistant against light, heat and other physical agents, leading to high level of dimensional stability, mechanical strength and chemical/solvent resistance (Bhattacharya *et al.*, 2009). Chemical cross-linking agents that are commonly utilized are glutaraldehyde, formaldehyde, acetaldehyde and other monoaldehydes. Formation of acetal bridges will occur when these cross-linking agents are used together with sulphuric acid, methanol or acetic acid (Hassan and Peppas, 2000).

Glutaraldehyde (GA) or 1,5-pentanedial ($\text{HOC}-(\text{CH}_2)_3\text{-COH}$) is widely employed in protein immobilization and cross-linking through amino groups which is suitable in promoting fixation and it is an inexpensive method (Beppu *et al.*, 2007). In addition, GA has advantages such as high activity of aldehyde groups and its readiness in forming Schiff's base with amino group of protein (Wang *et al.*, 2004). The mechanism takes place with nucleophilic attack by nitrogen in the amino group towards the carbon group of GA which replaces the oxygen of the aldehyde forming imine bond ($\text{C}=\text{N}$) (Berger *et al.*, 2004).

Unfortunately, Schiff bases are known to be unstable in acidic condition and easily break down into aldehyde and amine. In contrast, the one formed by the reaction of amino groups and GA has exhibited exceptional stability at extreme pH's and temperatures. There are various forms of GA even for specific and controlled reaction conditions. Besides, GA also has several different mechanisms of reaction that can take place simultaneously (Migneault *et al.*, 2004).

The properties of the cross-linked material may change with the density of the cross-linking agent such as water molecule diffusion and accessibility to the polymeric chain become difficult as the flexibility of the polymer chain is reduced.